

ON IMPEDANCE CONTROL FOR LANDING MECHANISMS ON COMETS AND PLANETS

Zisos Mitros,⁽¹⁾ Spyridon Garyfallidis,⁽²⁾ and Evangelos Papadopoulos⁽³⁾

National Technical University of Athens
Department of Mechanical Engineering – Control Systems Laboratory
9 Heroon Polytechniou Str., 15780, Athens, Greece
e-mail: ⁽¹⁾zmitros@gmail.com, ⁽²⁾sp.garyf@gmail.com, ⁽³⁾egpapado@central.ntua.gr

ABSTRACT

Recent successes of missions, such as the Rosetta, have increased the interest in the robotic exploration of other planets and asteroids. Although, in most landers passive landing systems are used, bouncing due to inappropriate descent speed and hardware malfunction have been observed in cases such as that of the Philae. In this paper, an impedance control law for an active landing gear is studied, which can increase the robustness to the speed of descent and to other miscalculations. Based on the proper selection of impedance parameters, bouncing can be avoided and a soft landing can be achieved for a range of descent speeds. Simulation results on Matlab/Simulink and Gazebo that validate the developed analysis are included. Conclusions and guidelines on the use of actuated landing mechanisms are discussed.

1. INTRODUCTION

Space exploration and human curiosity can be served by sending landers and space probes to distant planets and comets. The landers help scientists study comets, and learn about the history of the Solar System, or study planets, and find out if they can be inhabited. By contrast with impact probes, which make hard landing and are destroyed after reaching the surface, landers are required to make a soft landing in order to remain functional. These reasons have pushed space agencies worldwide to dedicate a significant amount of their budget to careful studies of the most critical part of a mission: the landing phase. NASA's Viking Mission to Mars was composed of two spacecrafts, Viking 1 and Viking 2, each consisting of an orbiter and a lander. The importance of Viking's landers arises from the fact that even to date, the Viking missions give our most complete view of Mars, [1]. One of the most important missions was the Rosetta mission led by the European Space Agency (ESA). Rosetta, a space probe, along with Philae, its lander module would be the first to study a comet. Despite the success of the mission and the first ever landing on a comet nucleus, during its landing, Philae bounced off the surface twice, leading to an uncontrolled touchdown, which left it at a non-optimal location and orientation, [2]. In the most recent ESA mission, the European space probe Schiaparelli may have crashed on Mars after suffering problems

releasing its parachute and firing its retrorockets to slow its descent. The exact reasons for this failure are under investigation.

Landing on small bodies is, in principle, very different to the landing on a planet or large moon due to the fact that the gravitational field may be weak and not homogeneous. Because of these reasons, special and often expensive descent and landing strategies are required. Despite extensive analysis prior to launch, complications during missions have been observed. Signal time delays make the communication and command difficult, which can be critical to the success of a mission, leading to the need of extensive analysis prior to launch of the mission. Lander capsizing or rebounding due to low gravity, inappropriate descent velocity and hardware malfunction are considerable threats to the success of a mission, [4]. Those are few of the problems that engineers face during the planning of the landing phase.

Landing mechanisms are mostly systems that present passive compliance in order to achieve a desired soft landing. Passive compliance utilizes mechanical compliance with no control time delay. However, they present limitations regarding their operation, [2]-[3]. Changes in the descent velocity due to the unknown gravitational field of a comet often lead to miscalculation of the passive elements i.e. springs and dampers of the landing gear. Apart from passive systems, recent works on landing also make use of active compliance systems, in order to minimize the impact forces and achieve soft landing, [5]. Active compliance is an important research topic in robotics, which can bring up many new ideas regarding the minimization of impacts and impulses during interactions. Impedance control is an example of active compliance control, which incorporates the use of a system model [6]. It can regulate the relationship between an end-effector and the interaction force by simply imposing impedance characteristics on the apparent behaviour of the system under study, [7]. A *Multiple Impedance Control* (MIC) law for a manipulator has been proposed and compared with other control strategies showing the ability both for free motions and contact tasks without switching control

modes, [8]. The MIC enforces a desired reference impedance on both the manipulator end-points and the manipulated object, and hence, an accordant motion of the manipulators and payload is achieved.

In this paper, a concept for the landing phase of a space mission based on active compliance is studied, which differs from the classic approach of using passive mechanisms. To control the landing gear, an impedance controller is developed to achieve the desired landing behaviour. The landing gear under study has two Degrees-of-Freedom (DOFs) per leg. The importance of the proper selection of the impedance parameters is shown. Simulation results on Matlab/ Simulink and Gazebo [12] are included that validate the proposed controller. Conclusions and guidelines on the use of actuated landing mechanisms are discussed.

2. LANDING SCENARIO AND DYNAMICS

A proposed scenario for landing consists of a lander spacecraft that is composed of six basic subsystems: the lander body, the bioshield cap and base, the aeroshell, the base cover with its parachute system and the landing gear. Without loss of generality, all the systems apart from the landing gear are modelled as a large lumped mass m_l . In this scenario, the lander will rest on a landing gear forming a tripod. Each leg of the tripod has two joints, arranged as shown in Figure 1. The first joint is at the hip while the second one is at the knee. All actuators are concentrated at the lander body to minimize the weight of each leg. Thanks to the symmetry that the tripod presents in this study, a single leg is studied along with the lander mass m_b that rests on that leg, which is taken as the third of the lander's mass, m_l . Making the assumption that the lander falls with zero pitch and taking into account the symmetry that the system presents; the lander body is able to move only in the y-axis as shown in Figure 1.

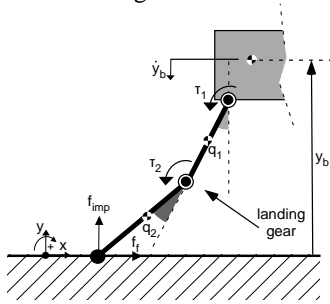


Figure 1. Lander model, showing one leg only.

As shown in Figure 1, the model consists of the mass m_b , describing the lander body seen by a leg, and one two-segment leg, with each segment being of mass m_i and moment of inertia (MoI) I_i about its Center of Mass (CoM) where $i \in \{1, 2\}$. Each segment CoM is in the middle of its length l_i . The leg segments are numbered starting from the ones hinged to the body using the subscript i . The hip and knee joints are driven by

actuators modelled as ideal torque sources τ_i .

In deriving the equations of motion, the employed generalized coordinates include the body CoM position vector in the inertial frame y_b and the angles of the two joints q_1, q_2 , as shown in Figure 1. Then, the equations of motion take the following form,

$$\mathbf{M}(\mathbf{q}) \cdot \ddot{\mathbf{q}} + \mathbf{C}(\mathbf{q}, \dot{\mathbf{q}}) = \boldsymbol{\tau} + \mathbf{J}^T \cdot \mathbf{f}_{\text{ex}} \quad (1)$$

where $\mathbf{q} = [y_b, q_1, q_2]$ represents the configuration space as described above, $\mathbf{M}(\mathbf{q})$ is a symmetric 3x3 mass matrix, $\mathbf{C}(\mathbf{q}, \dot{\mathbf{q}})$ is a 3x1 vector containing gravity, centrifugal and Coriolis terms, and the Jacobian \mathbf{J} resolves the external forces \mathbf{f} from the ground to joint torques. Those matrices can be found in the Appendix. Separating the actuated from the non-actuated generalized coordinates, the equations of motion can be expressed as follows,

$$\begin{bmatrix} \tilde{\mathbf{M}}_{11} & \tilde{\mathbf{M}}_{12} \\ \tilde{\mathbf{M}}_{21} & \tilde{\mathbf{M}}_{22} \end{bmatrix} \begin{bmatrix} \ddot{y}_b \\ \ddot{\mathbf{q}}_{\text{ac}} \end{bmatrix} + \begin{bmatrix} \tilde{\mathbf{C}}_1 \\ \tilde{\mathbf{C}}_2 \end{bmatrix} = \begin{bmatrix} f_b \\ \boldsymbol{\tau} \end{bmatrix} + [\mathbf{J}_1^T \quad \mathbf{J}_2^T] \mathbf{f}_{\text{ex}} \quad (2)$$

where the actuated coordinates are the angles of the two joints,

$$\mathbf{q}_{\text{ac}} = [q_1 \quad q_2]^T \quad (3)$$

and \mathbf{f}_{ex} is the external reaction force applied to the foot,

$$\mathbf{f}_{\text{ex}} = [f_{\text{imp}} \quad f_f]^T \quad (4)$$

where f_{imp} is the normal force and f_f is the friction. In this study, the thrusters on the lander's main mass are off i.e. $f_b = 0$. By eliminating \ddot{y}_b from the lower part of Eq. (2) using its upper part, the equation of motion in joint coordinate space can be obtained as follows

$$\mathbf{M}_g \ddot{\mathbf{q}} + \mathbf{C}_g = \mathbf{J}_g^T \mathbf{f}_{\text{ex}} + \boldsymbol{\tau} \quad (5)$$

where the matrices \mathbf{M}_g and \mathbf{J}_g are the generalized inertia matrix and the generalized Jacobian matrix, respectively, given by

$$\begin{aligned} \mathbf{M}_g &= \tilde{\mathbf{M}}_{22} - \tilde{\mathbf{M}}_{21} / \tilde{\mathbf{M}}_{11} \cdot \tilde{\mathbf{M}}_{12} \\ \mathbf{J}_g &= \mathbf{J}_2^T - \tilde{\mathbf{M}}_{21} / \tilde{\mathbf{M}}_{11} \cdot \mathbf{J}_1^T \\ \mathbf{C}_g &= \tilde{\mathbf{C}}_2 - \tilde{\mathbf{M}}_{21} / \tilde{\mathbf{M}}_{11} \cdot \tilde{\mathbf{C}}_1 \end{aligned} \quad (6)$$

Table 1. Nomenclature

| Symbol | Quantity |
|------------------|--|
| y_b | Lander CoM y-axis coordinate |
| q_1 | Hip angle |
| q_2 | Knee angle |
| x_f, y_f | Foot coordinates |
| l_1, I_1, m_1 | Characteristics of the link's first segment |
| l_2, I_2, m_2 | Characteristics of the link's second segment |
| F_{imp} | Ground force in vertical direction |
| F_f | Friction force in horizontal direction |
| τ_1 | Hip torque |
| τ_2 | Knee torque |
| m_f, b_f, k_f | Impedance Parameters |

Foot – ground interaction. To represent the interaction of the foot with the ground during touchdown realistically, the viscoelastic theory is employed. According to this theory, a compliant surface under impact can be modelled by a combination of lumped elements i.e. springs and dampers. A common impact model, which yields good results, is the Kelvin-Voigt (KV) model, [9]-[10]. Employing this model, the normal impact force f_{imp} is

$$f_{imp}(y_g, \dot{y}_g) = k_i \cdot y_g + b_i \cdot \dot{y}_g \quad (7)$$

where k_i and b_i are the stiffness and damping coefficients of the impact respectively and y_g is the penetration of the foot in the ground. As far as the friction is concerned, it can be modelled also as a spring-damper system between the x-coordinate of the foot and its projection to the ground before the touchdown; with k_{fr} , b_{fr} to be the stiffness and damping coefficients respectively of the friction force. The ground reactions must lie inside the leg friction cone, i.e.,

$$\left| \frac{f_f}{f_{imp}} \right| < \mu \quad (8)$$

where μ is the friction coefficient. Based on Eq.(8), the stiffness and damping coefficients of the friction force are selected.

3. IMPEDANCE CONTROLLER DESIGN

An impedance filter for foot control is introduced aiming in a desired landing behaviour,

$$\begin{aligned} m_{fx} \cdot \ddot{\tilde{x}} + b_{fx} \cdot \dot{\tilde{x}} + k_{fx} \cdot \tilde{x} &= 0 \\ m_{fy} \cdot \ddot{\tilde{y}} + b_{fy} \cdot \dot{\tilde{y}} + k_{fy} \cdot \tilde{y} &= -f_{ex,y} \end{aligned} \quad (9)$$

where \tilde{x} is the relative position of the foot's x-coordinate x_f to the position of the lander base x_b and \tilde{y} is the relative position of the foot's y-coordinate y_f to the position of the lander base y_b , before and after the landing i.e.,

$$\begin{aligned} \tilde{x} &= (x_{b0} - x_{f0}(q_{10}, q_{20})) - (x_b - x_f(q_1, q_2)) \\ \tilde{y} &= (y_{b0} - y_{f0}(q_{10}, q_{20})) - (y_b - y_f(q_1, q_2)) \end{aligned} \quad (10)$$

The coordinates of the foot are connected to the coordinates of the base as follows,

$$\begin{aligned} x_f &= x_b - l_1 \cdot \sin q_1 - l_2 \cdot \sin(q_1 + q_2) \\ y_f &= y_b - l_1 \cdot \cos q_1 - l_2 \cdot \cos(q_1 + q_2) \end{aligned} \quad (11)$$

The relative acceleration of the foot and the lander body expressed in the joint angle acceleration is:

$$\begin{pmatrix} \ddot{\tilde{x}} \\ \ddot{\tilde{y}} \end{pmatrix} = \begin{pmatrix} a_{11} & a_{12} \\ a_{21} & a_{22} \end{pmatrix} \cdot \begin{pmatrix} \ddot{q}_1 \\ \ddot{q}_2 \end{pmatrix} + \begin{pmatrix} n_1 \\ n_2 \end{pmatrix} \quad (12)$$

where a_{ij} and n_i , $\{i, j\} \in \{1, 2\}$ are functions of the joint angles and speeds. In the scheme of the proposed impedance control, the angular acceleration of each

joint of the leg through the use of Eq. (9)- (12) is controlled as follows:

$$\begin{pmatrix} \ddot{q}_1^d \\ \ddot{q}_2^d \end{pmatrix} = \begin{pmatrix} m_{fx} a_{11} & m_{fx} a_{12} \\ m_{fy} a_{21} & m_{fy} a_{22} \end{pmatrix}^{-1} \begin{pmatrix} -b_{fx} \dot{\tilde{x}} - k_{fx} \tilde{x} - m_{fx} n_1 \\ -f_{ex,y} - b_{fy} \dot{\tilde{y}} - k_{fy} \tilde{y} - m_{fy} n_2 \end{pmatrix} \quad (13)$$

where the superscript d denotes the desired quantity. Substituting Eq. (13) in Eq. (5), the input torques are obtained as follows,

$$\boldsymbol{\tau}_d = -\mathbf{J}_g^T \mathbf{f}_{ex} + \mathbf{M}_g \ddot{\mathbf{q}}_d + \mathbf{C}_g \quad (14)$$

where $\boldsymbol{\tau}_d$ are the torques applied by the controller.

4. SELECTION OF IMPEDANCE PARAMETERS

To control properly the lander's leg and achieve a soft landing, the impedance parameters must be selected carefully in accordance to the descent velocity. Generally, soft landing is consisted by small bounces that does not jeopardize the final touchdown of the lander in the desired position or the functionality of the lander's hardware. In the most desirable case, no bounces take place. As a result, the impedance parameters must be selected in such a way that small or even zero bounces occur based on the changes on the descent velocity, that in a real scenario may be due to hardware malfunction or miscalculations on the gravitational field of the space body on which the landing will take place. However, an analytical solution for the selection of these parameters is difficult to be obtained because of the large number of parameters involved. To investigate possible sets of impedance parameters that provide a soft landing, an algorithm that searches for proper values of those parameters based on a desired behaviour and descent velocity, was created [11]. The inputs of the algorithm are the maximum joint motor torques, the maximum bounce height of the lander's main mass, as well as the search range for the impedance parameters values that the algorithm has to explore. The results of the algorithm for $\tau_1 < 100$ Nm, $\tau_2 < 100$ Nm and $y_b < 0.8$ m, are shown in Figure 2. The parameter selection process begins with choosing a desired descent velocity.

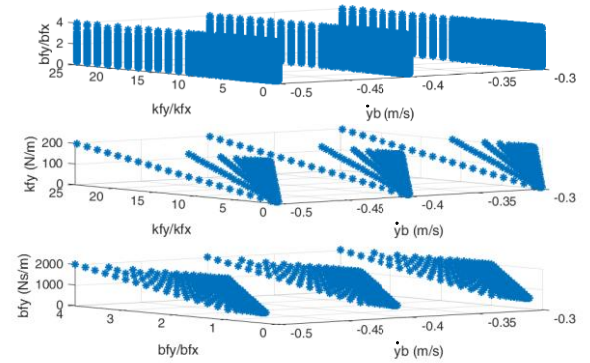


Figure 2. Impedance filter parameters as a function of descent velocity.

Using Figure 2a, one can select the ratios k_{fy}/k_{fx} and b_{fy}/b_{fx} , as functions of the descent velocity that will be used on the scenario under study. Those ratios can be selected in such a way that for the same ratios, more than one velocity will provide the desired behavior. Based on these ratios and the velocity, the impedance parameters k_{fy} and b_{fy} are selected using Figure 2b and Figure 2c. Therefore, k_{fx} and b_{fx} are also indirectly defined, since their ratio has been selected. Note that the impedance parameters m_{fx} and m_{fy} have been selected equal to $m_{fx} = 10\text{kg}$ and $m_{fy} = 10\text{kg}$ in order to minimize the computational time and simplify the analysis of the algorithm's results.

To obtain a better picture of how each parameter affects the accomplishment of landing as well as see how robust the controller is regarding the change of the descent velocity, Figure 3 was created by keeping constant all the impedance parameters apart from k_{fy} . As can be seen, by increasing k_{fy} , the range of acceptable values of descent velocity that provide soft landing decreases. That seems reasonable as by increasing k_{fy} the virtual spring between the lander's main mass and the foot becomes more and more stiff and thus it can absorb less energy transferred due to the contact of the foot to the ground. Similar figures and conclusions can be obtained for the other parameters. Furthermore, it is observed from graphs similar to those of Figure 2 that for the impedance parameters of the Case A of Table 2, the velocity that provides a soft landing is $\dot{y}_b = [-1.25, -0.55] \cup \{-0.45\}, \{-0.4\}$ where $[\dot{y}_b] = \text{m/s}$. Based on this range, it can be concluded that miscalculations on the descent velocity can be tolerated by the controller and thus lead to avoidance of mission failure. In the case, that the descent velocity is out of the aforementioned range, proper impedance parameters can be obtained from graphs like the one of Figure 2. Moreover, the robust of the controller due to changes on the descent velocity can be shown also from the Figure 3, as for the same k_{fy} more than one velocities are acceptable.

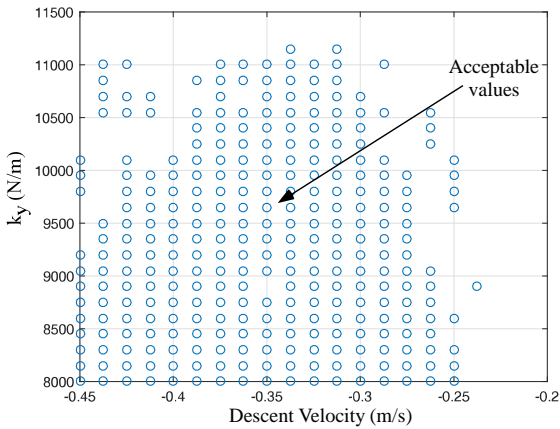


Figure 3. Range of descent velocities as a function of the impedance filter vertical stiffness k_{fy} .

Table 2. Data for simulation runs.

| Impedance Parameters | A | B |
|----------------------|------|------|
| m_{fx} (kg) | 10 | 10 |
| m_{fy} (kg) | 10 | 10 |
| b_{fx} (Nm) | 1000 | 8 |
| b_{fy} (Nm) | 1000 | 8 |
| k_{fx} (N/m) | 8 | 1000 |
| k_{fy} (N/m) | 8 | 1000 |

5. SIMULATION RESULTS

To examine the validity of the analysis and show the importance of the impedance parameters' proper selection, a series of simulations using MATLAB/Simulink were run. As the lander descends due to initial velocity and gravity, it touches the ground and impact forces are developed and calculated using the KV model. As the simulation advances, the velocity of the foot in contact with the ground, as well as its penetration in it, are calculated. These values are fed back to the contact model and the impact compression force is calculated, which pushes the leg upwards. Based on that force and the selected impedance parameters with the aforementioned method, it is possible to keep the foot in contact with the ground by applying desirable torques through the use of the impedance controller.

To create a realistic series of simulations, values close to those of missions in planets and comets were used. In the scenario under study the spring that models the ground stiffness is selected as $k_i = 10000 \text{ N/m}$ and its damping equal to $b_i = 1000 \text{ Ns/m}$. The lander's main body mass was selected as $m_b = 30\text{kg}$, while the leg's characteristics are $l_1 = 1\text{m}$, $I_1 = 10\text{kgm}^2$, $m_1 = 10\text{kg}$ and $l_2 = 0.5\text{m}$, $I_2 = 10\text{kgm}^2$, $m_2 = 5\text{kg}$. The acceleration of gravity was chosen equal to $g = 1 \text{ mm/s}^2$. Generally, the lander can begin its fall either from an altitude of a few kilometres similar to Philae's mission, or of a few meters in the case that a parachute or a sky crane is employed. In Table 2, the values of the impedance parameters that were used in the simulations for two cases, namely A and B, are shown. The impedance parameters that result in a soft landing where chosen using graphs like Figure 2 and according to the methodology of Section. 4.

Next, we study the cases of a failure in descent and a case of successful soft landing.

Bouncing of the lander – Failure of the mission: In the case that the impedance parameters are chosen arbitrary, bouncing of the lander that may lead to its escape from the influence of the gravitational field or landing in a non-optimal area after many bounces, can be observed. As shown in Figure 4, it can be observed that by using Case B random impedance parameters given in Table 2,

the lander bounces and escapes the gravitational field; leading to failure of the mission.

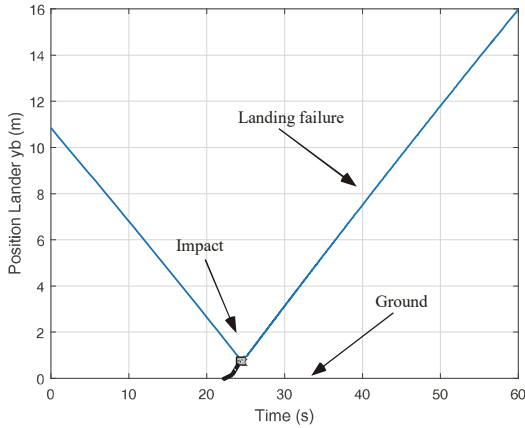


Figure 4. Bouncing of the lander – Mission failure.

Soft landing: Using the methodology of Section 4, proper impedance parameters for a soft landing can be obtained. As shown in Figure 5, the lander is ejected from a height of $y_{b0} = 10.85\text{m}$. The descent velocity is $\dot{y}_{b0} = -0.4\text{m/s}$ and the leg touches the ground at $t_{touch} = 24.29\text{s}$. Using the Case A impedance parameters of the Table 2, torques according to Eq. (14) are exerted by the leg joint motors. Based on the proper selection of the impedance parameters, it can be seen from the Figure 5 that the lander’s main mass is not lifted while the Figure 6b shows that the foot bounces for some millimetres and after that remains steady and attached to the ground. From the Figure 6a, it can be seen that slip is appeared which is less than 2mm. Such a value is considered to be negligible for the way that friction was modelled.

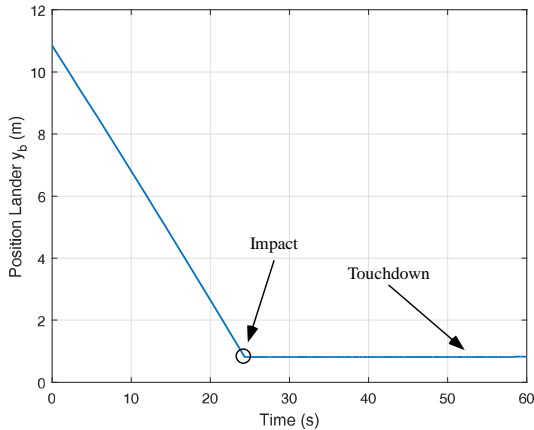


Figure 5. Position of the lander’s main mass m_b

As far as the exerted torques are concerned, Figure 7 shows that their peak is reached at $t_{touch} = 25.3\text{s}$, right after the touchdown and at the moment that the impact force reaches its maximum value. Those values are $\tau_1 = 486\text{ Nm}$ and $\tau_2 = 875.5\text{ Nm}$. After the moment $t = 27.3\text{s}$, it can be observed that the torques are small in magnitude and are reduced slowly as time progresses

due to the small damping factor that is presumed and the fact that the impact is modelled as a spring- damper system. After a small duration of time the torques are close to zero and those are necessary to hold the leg’s weight. Those torques are responsible for keeping the leg in the desired position. The large magnitude of torques during the touchdown can be reduced by the use of series elastic actuators or passive compliance.

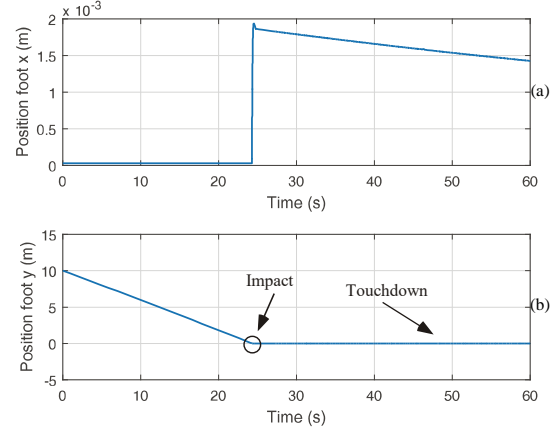


Figure 6. Position of the foot.

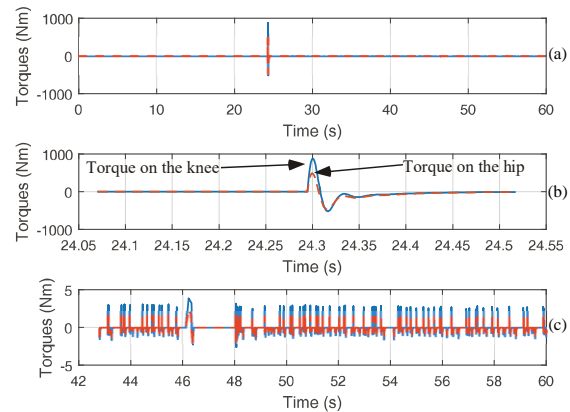


Figure 7. Controller’s torques.

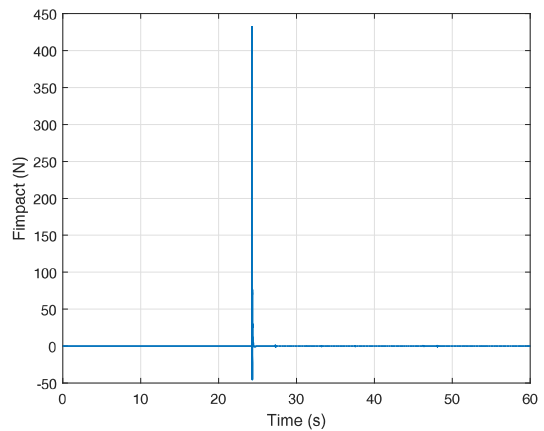


Figure 8. Impact force during touchdown.

6. IMPLEMENTATION OF ANALYSIS IN GAZEBO

To further examine the controller's response, but also to take a step closer to an actual hardware implementation, the proposed controller design was applied and tested on a Gazebo model. The Robot Operating System (ROS) was selected as the platform to implement and connect the controller to the model for two main reasons. First, it is the platform that is employed commonly, and at CSL, for most robotic applications. Second, writing code for simulation purposes is not different from writing code for real hardware experiments. With a real hardware test in mind, running a simulation in Gazebo allows us to debug the actual software, with minor interface differences, so the only thing missing is the hardware implementation. As a first stage it was decided to simulate the single leg model that was tested in MATLAB/Simulink and see if the results would coincide. For that purpose the model seen in Figure 9 was created.

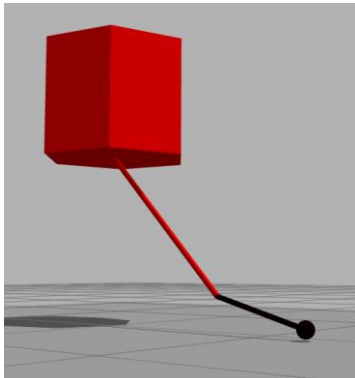


Figure 9. The single leg approximation of the lander in the Gazebo environment.

For the same parameters (ground contact stiffness and damping, gravitational pull, impedance gains and inertial characteristics), the simulation results for one of the legs were actually close to those that were received from MATLAB/Simulink. Both simulations show successful landing and stabilization about 40 seconds after the first impact (see Figure 5 and Figure 10), while there are some small differences concerning the maximum rebound, steady state body height and joint torques. The impact forces are almost identical, see Figure 8 and Figure 12. Note that for computational reasons the lander was dropped from 0.01 instead of 10 m, with the initial velocity that corresponds to $g = 0.001 \text{ m/s}^2$ and $\dot{y}_b = -0.4 \text{ m/s}$ when at 10m.

The aforementioned differences can be explained if one considers the tools that MATLAB offers, like the potential for proper differentiation. In Gazebo one essentially receives sensor measurements and has to differentiate using the control loop's time step, a method that inserts a great deal of noise. That noise was dealt with, to a certain extent, using filters but it cannot

be eliminated completely. This can adequately explain the differences in the torque values (see Figure 7 and Figure 11). The differences in the height values could be a result of different approaches of the friction model between the two simulations. In Simulink the friction force was exerted by a simulated spring-damper, while in Gazebo, an approximation of the friction cone model was used, causing minimum slippage, and therefore slightly augmented steady state height. Another minor difference between the two simulations is the addition of a ball toe, in order to stabilize the toggling contact that was detected by the force-torque sensor in Gazebo. In any case the differences between the results are deemed to be insignificant.

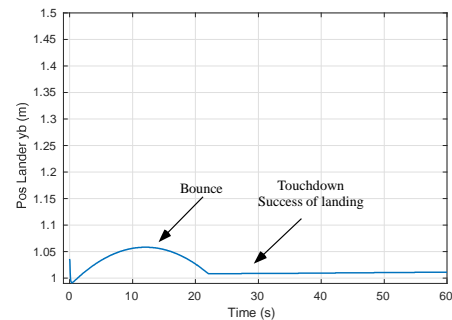


Figure 10. Position of the lander's main mass m_b from Gazebo.

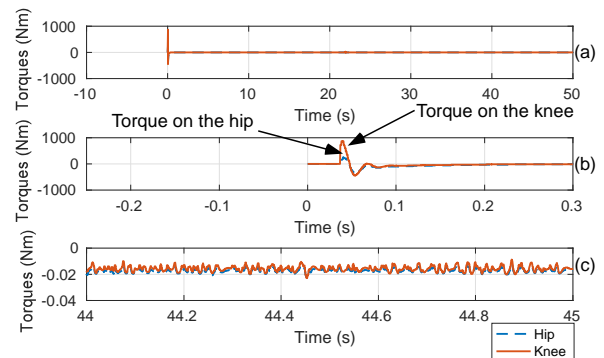


Figure 11. Torques from the controller

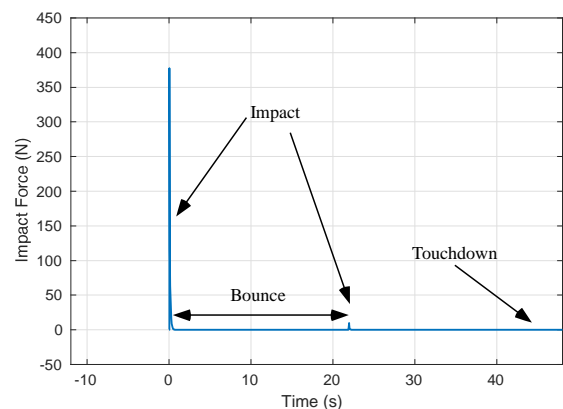


Figure 12. Impact force during touchdown as derived from Gazebo.

In addition to the simplified model of a single leg approximation that was tested in both simulation platforms, and in order to test the controller in a more realistic scenario, it was decided to also examine its response on a more realistic tripod lander model, see Figure 13. This approach neglects any leg placement, localization, as well as balance issues that might occur, problems that are too complicated to be handled by a single algorithm and that would be dealt with by different elements of software in a real lander.

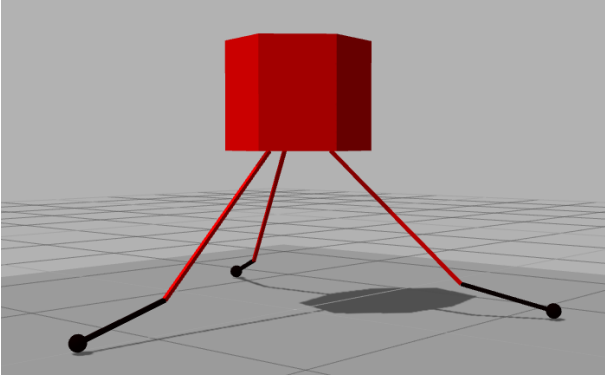


Figure 13. The tripod lander in the Gazebo environment.

The controller shows good potential even in the case of a tripod lander, a more complicated case, with results and functionality with good resemblance to those of the single leg model. In Figure 14 one can observe that the body stabilizes in a similar fashion with the single leg model, only slightly lower than before at 1m, and about at the same time (22 – 24s).

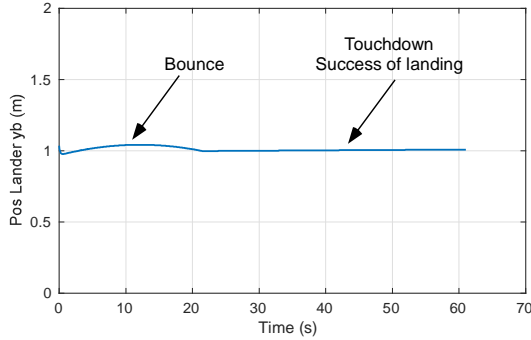


Figure 14. Position of the tripod lander's main mass m_b from Gazebo

7. CONCLUSION AND FUTURE WORK

In this paper, the critical phase of landing of a tripod lander with two DoFs in each leg was considered. The leg's motors are under impedance control in order to achieve a soft landing. An analytical model of the landing scenario was created in MATLAB/Simulink as proof of concept, in order to show the importance of the proper selection of impedance parameters to the mitigation or even avoidance of bouncing. Based on the

simulations that were presented in this paper, it can be concluded that active compliance can not only reduce bounces and their height but also ensure a successful landing in the case that the descent velocity is not the one that was intended to be. Moreover, to further examine the controller's functionality in real hardware in the future, the proposed controller design was applied and tested on a Gazebo model. In the future, experiments with an experimental scale lander regarding the validation of the impedance controller are to be conducted.

8. APPENDIX

The mass matrix in (2) is as follows,

$$M_{11} = m_1 + m_2 + m_b$$

$$M_{12} = (l_{c1} \cdot m_1 + l_1 \cdot m_2) \cdot \sin(q_{11}) + a_{c2} \cdot m_2 \cdot \sin(q_{11} + q_{12})$$

$$M_{13} = l_{c2} \cdot m_2 \cdot \sin(q_{11} + q_{12})$$

$$M_{21} = (l_{c1} \cdot m_1 + l_1 \cdot m_2) \cdot \sin(q_{11}) + l_{c2} \cdot m_2 \cdot \sin(q_{11} + q_{12})$$

$$M_{22} = I_1 + I_2 + l_{c1}^2 \cdot m_1 + (l_1^2 + l_{c2}^2) \cdot m_2 + 2 \cdot l_1 \cdot l_{c2} \cdot m_2 \cdot \cos(q_{12})$$

$$M_{23} = I_2 + l_{c2}^2 \cdot m_2 + l_1 \cdot l_{c2} \cdot m_2 \cdot \cos(q_{12})$$

$$M_{31} = l_{c2} \cdot m_2 \cdot \sin(q_{11} + q_{12})$$

$$M_{32} = I_2 + a_{c2}^2 \cdot m_2 + l_1 \cdot l_{c2} \cdot m_2 \cdot \cos(q_{12})$$

$$M_{33} = I_2 + l_{c2}^2 \cdot m_2$$

The $\mathbf{C}(\mathbf{q}, \dot{\mathbf{q}})$ which is a 3x1 vector containing gravity, centrifugal and Coriolis terms in (2) is as follows,

$$C_{11} = g \cdot (m_1 + m_2 + m_b) + (l_{c1} \cdot m_1 + l_1 \cdot m_2) \cdot \cos(q_{11}) \cdot (\dot{q}_{11})^2 + l_{c2} \cdot m_2 \cdot \cos(q_{11}) \cdot \cos(q_{12}) \cdot ((\dot{q}_{11}) + (\dot{q}_{12}))^2 +$$

$$(-1) \cdot l_{c2} \cdot m_2 \cdot \sin(q_{11}) \cdot \sin(q_{12}) \cdot ((\dot{q}_{11}) + (\dot{q}_{12}))^2$$

$$C_{21} = g \cdot (l_{c1} \cdot m_1 + l_1 \cdot m_2) \cdot \sin(q_{11}) + l_{c2} \cdot g \cdot m_2 \cdot \sin(q_{11} + q_{12}) + (-1) \cdot l_1 \cdot l_{c2} \cdot m_2 \cdot \sin(q_{12}) \cdot (\dot{q}_{12}) \cdot (2 \cdot (\dot{q}_{11}) + (\dot{q}_{12}))$$

$$C_{31} = l_{c2} \cdot m_2 \cdot (g \cdot \sin(q_{11} + q_{12}) + l_1 \cdot \sin(q_{12}) \cdot (\dot{q}_{11})^2)$$

where $l_{ci} = l_i/2$ for $i=\{1,2\}$. The Jacobian shown in (2) is as follows,

$$\mathbf{J}^T = \begin{bmatrix} 1 & 0 \\ l_2 \sin(q_{11} + q_{12}) + l_1 \sin(q_{11}) & -(l_2 \cos(q_{11} + q_{12}) + l_1 \cos(q_{11})) \\ l_2 \sin(q_{11} + q_{12}) & -(l_2 \cos(q_{11} + q_{12})) \end{bmatrix}$$

9. ACKNOWLEDGEMENTS

This work was partially supported from the European Commission through contract FP7-SME-2013/605420 (HexaTerra).

10. REFERENCES

1. Ezell, E.C., & Ezell, L.N., (1984). *On MARS Exploration of the Red Planet 1958-1978* The NASA History Series, Scientific and Technical Information Branch, National Aeronautics and Space Administration, Washington, D.C.
2. Hohe, L., (2009) "Surface elements and landing strategies for small bodies missions – Philae and beyond" *Advances Space Research* 44 pp, 847-858.
3. Rogers, F, W., (1972) "*APOLLO Experience Report – Lunar Module Landing Gear Subsystem*" NASA Technical Note, Washington, D. C.
4. Muñoz, P., et al (2015) "Rosetta Navigation During Lander Delivery Phase and Reconstruction of Philae Descent Trajectory and Rebound" *25th International Symposium on Space Flight Dynamics*.
5. www.space.com/news/2013/03/26/landing-leg
6. Moosavian, S. Ali A. and Papadopoulos, E. (1998) "Multiple Impedance Control for Object Manipulation," *Int. Conf. on Intelligent Robots and Systems (IROS '98)*, Victoria, BC, Canada, October 1998.
7. N. Hogan (1985), "Impedance Control: an approach to manipulation- A three part paper," *ASME Journal of Dynamic Systems, Measurement, and Control*, vol. 107, pp. 1-24.
8. Moosavian, S. Ali A. and Papadopoulos, E (2010) "Cooperative object manipulation with contact impact using multiple impedance control" *Int. Journal of Control, Automation, and Systems*, 8 (2), pp. 314–327.
9. Gilardi, G. and Sharf, I. (2002). "Literature Survey of Contact Dynamics Modelling," *Mech. & Machine Th.*, 37(10), pp. 1213-1239.
10. Stronge, W. J. (2000). *Impact Mechanics*, Cambridge University Press, ISBN 9780521602891.
11. Mitros, Z., Paraskevas, I., and Papadopoulos, E., "On Robotic Impact Docking for On Orbit Servicing", *24th Mediterranean Conference on Control and Automation*, 21-24 June 2016, Athens, Greece.
12. Koenig, N., Howard "Design and use paradigms for Gazebo, an open-source multi-robot simulator", *Int. Conf. on Intelligent Robots and Systems (IROS '04)*, Sendai, Japan